Nanoscopic control and quantification of enantioselective optical forces

Yang Zhao[1]*, Amr A. E. Saleh[1,2], Marie Anne van de Haar[3], Brian Baum[1], Justin A. Briggs[4], Alice Lay[4], Olivia A. Reyes-Becerra[1] and Jennifer A. Dionne[1]*

Circularly polarized light (CPL) exerts a force of different magnitude on left- and right-handed enantiomers, an effect that could be exploited for chiral resolution of chemical compounds[1-5] as well as controlled assembly of chiral nanostructures[6,7]. However, enantioselective optical forces are challenging to control and quantify because their magnitude is extremely small (sub-piconewton) and varies in space with sub-micrometre resolution[2]. Here, we report a technique to both strengthen and visualize these forces, using a chiral atomic force microscope probe coupled to a plasmonic optical tweezer[8-13]. Illumination of the plasmonic tweezer with CPL exerts a force on the microscope tip that depends on the handedness of the light and the tip. In particular, for a left-handed chiral tip, transverse forces are attractive with left-CPL and repulsive with right-CPL. Additionally, total force differences between opposite-handed specimens exceed 10 pN. The microscope tip can map chiral forces with 2 nm lateral resolution, revealing a distinct spatial distribution of forces for each handedness.

Chiral structures, which are non-superimposable with their mirror images, abound in nature at every size scale[14,15] and have distinct functions that emerge from their structure. In molecular biology, for example, enantiomers can exhibit distinct interactions with cellular binding sites, resulting in beneficial or detrimental effects based on the molecular handedness. Recently, it has been shown that the formation and separation of chiral compounds can be controlled with light[3,7,16]. However, enantioselective optical forces are exceedingly weak, scaling with the volume of the sample. For nanoscale specimens, the predicted forces are on the sub-piconewton scale. Moreover, enantioselective optical forces are often linked with evanescent[3,17] or superchiral[18] fields, with rapidly varying spatial distributions on the sub-micrometre scale. To strengthen and visualize these forces, we combine a plasmonic optical tweezer with a chiral atomic force microscope (AFM) probe. Our technique, termed chiral optical force microscopy (COFM), is shown in Fig. 1a. We illuminate the tweezer from the bottom with controlled polarization states of light and scan the chiral AFM tip across the top.

In conventional AFM studies, force measurements are performed either with the tip in contact with the sample[19,20] or in tapping mode[21-24]. Instead, we use a quasi-noncontact method to increase the sensitivity and range of forces that can be measured, as illustrated in Supplementary Figs 1 and 2 (see Methods and Supplementary Note 1 for details). To locate the sample surface and thus fix the tip at a precise z-height above the tweezer, a non-oscillating tip first approaches the sample surface and then, upon reaching the surface, retracts to a specified height. We then modulate the intensity of the incident light through the plasmonic tweezer at a frequency

matching the cantilever's natural resonance, but much lower than the optical frequency of the illumination. This low-frequency modulation significantly improves the single-to-noise ratio and enables precise measurement of the cantilever deflection and thus the optical forces.

The coaxial plasmonic aperture functions as an optical tweezer that both enables precise control of the optical chirality density and enhances enantioselective optical forces[25-27]. Additionally, the resonance of the aperture can be easily tuned to the near-infrared regime, where biological samples have minimal absorption. We use numerical simulations (finite-difference–time-domain (FDTD), Lumerical) to optimize the aperture geometry for transmission at ~770 nm, in the near-infrared window most desirable for potential bio-applications (Figs 1c and 2a). As shown in Fig. 1b, our optimized plasmonic nano-aperture consists of a 60 nm dielectric (air) ring embedded in a 220-nm-thick gold film (see Methods for fabrication details). It is patterned with a concentric bull's-eye grating to boost the transmission, thus increasing the near-field optical forces, and to narrow the angular spread of the transmitted beam[25,28]. White-light transmission measurements confirm the transmission peak at ~770 nm, corresponding to the fundamental Fabry–Pérot resonance of the aperture (Fig. 2a).

Before probing the plasmonic tweezer with a chiral AFM tip, we use an achiral tip to measure the optical forces emanating from the aperture. With a fixed tip–aperture separation of 50 nm and the tip parked in one position over the dielectric channel (Supplementary Fig. 3), we illuminate the tweezer at 770 nm with unpolarized light and toggle the source on and off with a rate far below that of the optical resonance. Forces of 55.3 ± 3.9 pN are measured with an achiral silicon AFM probe and correspond with the on/off pattern of the laser, confirming their optical origin (Fig. 2b). We then repeat the same measurement at an off-resonance wavelength of 660 nm (Fig. 2c), and the measured force again follows the illumination pattern of the laser. However, this force has a mean value of 35.8 ± 4.7 pN, ~40% lower compared to forces on resonance.

By sweeping the wavelength of the incident laser, we observe that the optical forces on the tip clearly follow the coaxial resonance (Fig. 2d). To determine the background signal, we repeat the same measurement at a location away from the aperture on the gold surface. As expected, the background signal does not show any spectral peaks (Fig. 2d). However, it does trend upwards at shorter wavelengths, corresponding to the optical absorption of the gold film. These results confirm that our spectroscopic force measurement has sufficient sensitivity to measure optical forces originating from our plasmonic optical tweezer.

To explore the effect of circularly polarized light (CPL), we illuminate our plasmonic optical tweezer with left- and right-handed

[1]Department of Materials Science and Engineering, Stanford University, Stanford, California 94305, USA. [2]Department of Engineering Mathematics and Physics, Faculty of Engineering, Cairo University, Giza, Egypt. [3]FOM Institute AMOLF, Science Park 104, 1098 XG Amsterdam, The Netherlands. [4]Department of Applied Physics, Stanford University, Stanford, California 94305, USA. *e-mail: yangzhao@stanford.edu; jdionne@stanford.edu
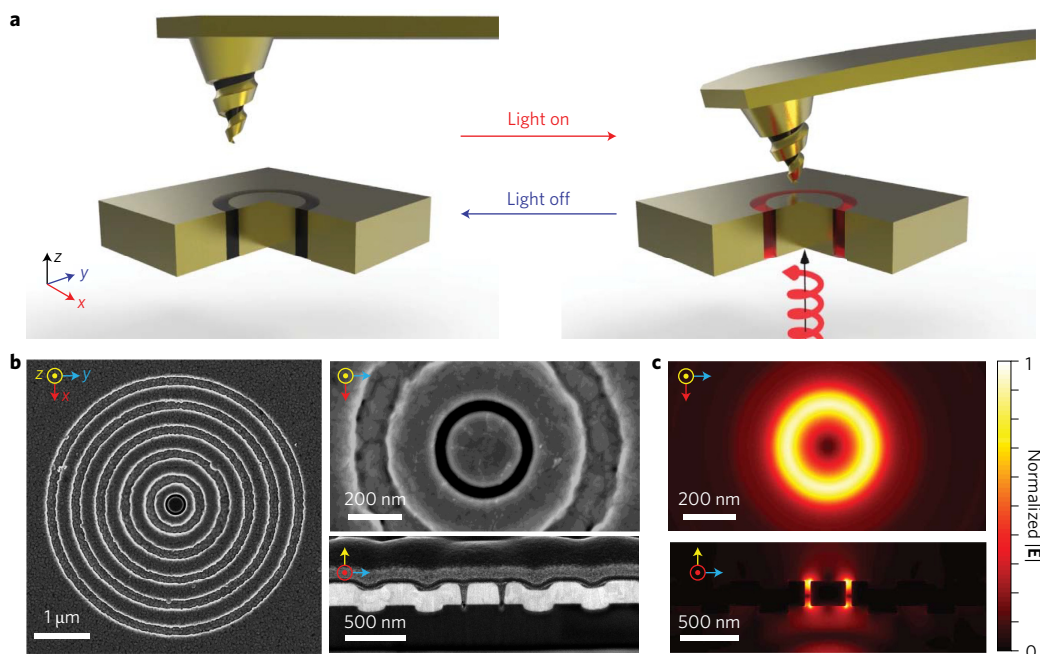
Figure 1 | Schematic, microscopic images, and simulations. a, Schematic illustration of enantioselective force mapping, where CPL illuminates a coaxial nano-aperture made of gold. **b**, Scanning electron microscope (SEM) images of grating-flanked coaxial nano-aperture. **c**, FDTD (Lumerical) simulations of the field distribution on resonance.
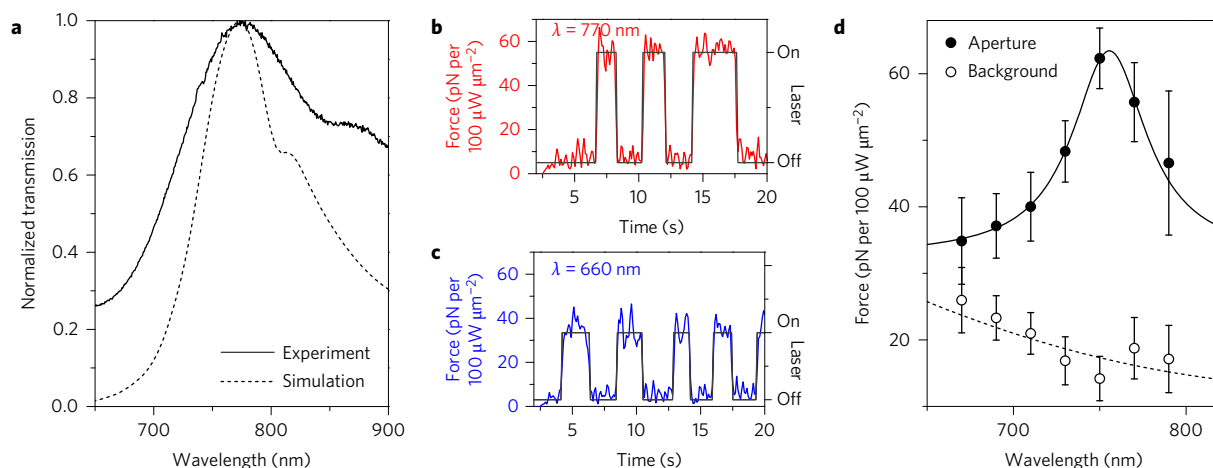

Figure 2 | Spectroscopically measured optical forces with an achiral tip. a, Normalized transmission spectra of the grating-flanked coaxial aperture shown in Fig. 1b. The dotted curve is from a numerical simulation (FDTD, Lumerical), and the solid curve is from experimental measurements. The shoulder of the spectrum at longer wavelengths (~825–875 nm) comes from the converging beam interacting with the grating. The blue and red dashed lines highlight wavelengths of 660 and 770 nm, respectively. **b**, Measured optical force when the incident laser is at 770 nm, near the resonance of the coaxial aperture. The laser is manually toggled on and off (black line) to confirm the fidelity of the measurement. **c**, Measured optical force away from the coaxial resonance at 660 nm. **d**, Spectroscopic measurement of optical forces at the aperture and away from the aperture, where the on-aperture measurement follows the spectrum of the aperture. Error bars represent standard deviations of measured forces at each wavelength. Solid and dashed curves are Lorentzian and polynomial fits, respectively.

CPL and then probe the transmitted near fields as a function of tip–aperture separation with the same achiral AFM tip (Fig. 3a). Figure 3c shows that the forces resulting from left- and right-CPL closely follow each other with the same spatial decay, indicating that the optical forces exerted on this AFM tip are nearly indistinguishable. The small difference between the forces induced by left- and right-CPL arises from the slightly asymmetric shape of the tip (Fig. 3a), which imparts very weak chirality[29].

To quantify the enantioselective forces acting on a chiral specimen, we introduce structural chirality in the probe by first depositing a thin

metallic film on the AFM tip and then using a focused ion beam to mill a spiral pattern with a period of $p = 155$ nm (Fig. 3b). Both left-handed (L) and right-handed (R) tips are patterned. The following results describe the detailed response of a gold L spiral tip, while Supplementary Notes 5 and 6 describe the response of the R spiral tip as well as tips made of non-plasmonic materials (Supplementary Figs 5–7). During the force measurement, the spiral tip acts as a chiral specimen that interacts with the local electromagnetic fields. Although the tip is inherently non-magnetic (that is, with a relative permeability of $\mu_r = 1$), CPL induces a circulating current due to the
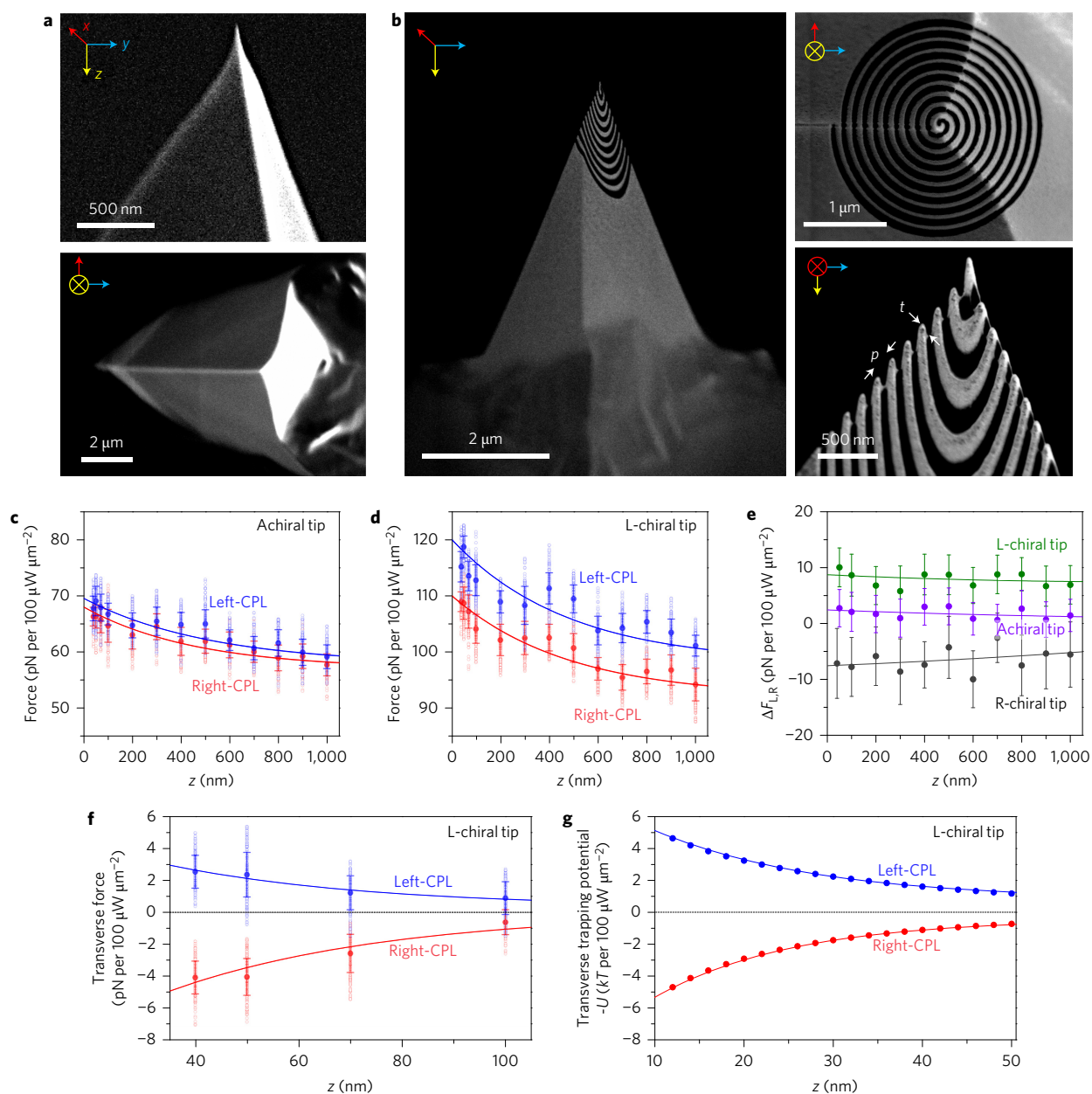
Figure 3 | Enantioselective optical forces with achiral and chiral tips. a, SEM images of an achiral silicon tip. **b**, SEM images of a chiral tip, which is made with focused ion beam milling (see Methods). Thickness, t, of the gold coating is ∼35 nm; period, p, of the spiral is ∼155 nm. **c**, Measured optical forces using the achiral tip with left-handed (blue) and right-handed (red) CPL at 750 nm. **d**, Measured optical force using the L-chiral tip with left-handed (blue) and right-handed (red) CPL. **e**, Comparison of the enantioselectivity in the measured forces (difference in the forces with left- and right-handed illumination), with both achiral and chiral tips. **f**, Measured transverse forces with the L-chiral tip, with left-handed (blue) and right-handed (red) CPL illumination. In all panels, open dots are raw data, filled dots are mean values, and error bars show standard deviations. Solid curves in **c**, **d** and **f** are fitted with exponential decay equations, and solid curves in **e** are fitted with polynomial equations. **g**, Simulated transverse trapping potentials exerted from the coaxial aperture on an L-chiral nanoparticle with size comparable to the AFM tip radius. Note that we plot the negative of the trapping potential to emphasize the trend being similar to the measurements.

structural chirality[30]. The resulting magnetic dipole moment interacts with the electric dipole moment, giving rise to an additional force that is proportional to the chirality of the specimen. For left- versus right-handed enantiomers, this additional chiral force is opposite in sign (see Supplementary Note 8 for a full theoretical description).

To measure the enantioselective optical force on our L-chiral tip, we illuminate the aperture with left- and right-CPL and probe different z-heights above the sample. As shown in Fig. 3d, the force resulting from left-CPL is significantly larger than that resulting from right-CPL. Our COFM set-up enables us to quantify the enantiomeric force differences at each z position over the sample. Figure 3e

shows that a differential force of up to 10 ± 3.5 pN is observed on the L-chiral tip, compared to 2.7 ± 3.3 pN observed with the achiral tip and up to −9.9 ± 5.1 pN with the R-chiral tip. Such differential forces also indicate that optical forces exerted through this achiral coaxial aperture can selectively trap a specimen based on its chirality.

We also find that the transverse forces exerted by left- and right-CPL have opposite signs as a function of z-height. Figure 3f shows that a chiral specimen placed at a given z-height above the aperture will be pulled towards the aperture when exposed to left-CPL, but pushed away when exposed to right-CPL. Indeed, FDTD simulations confirm that left- and right-CPL,
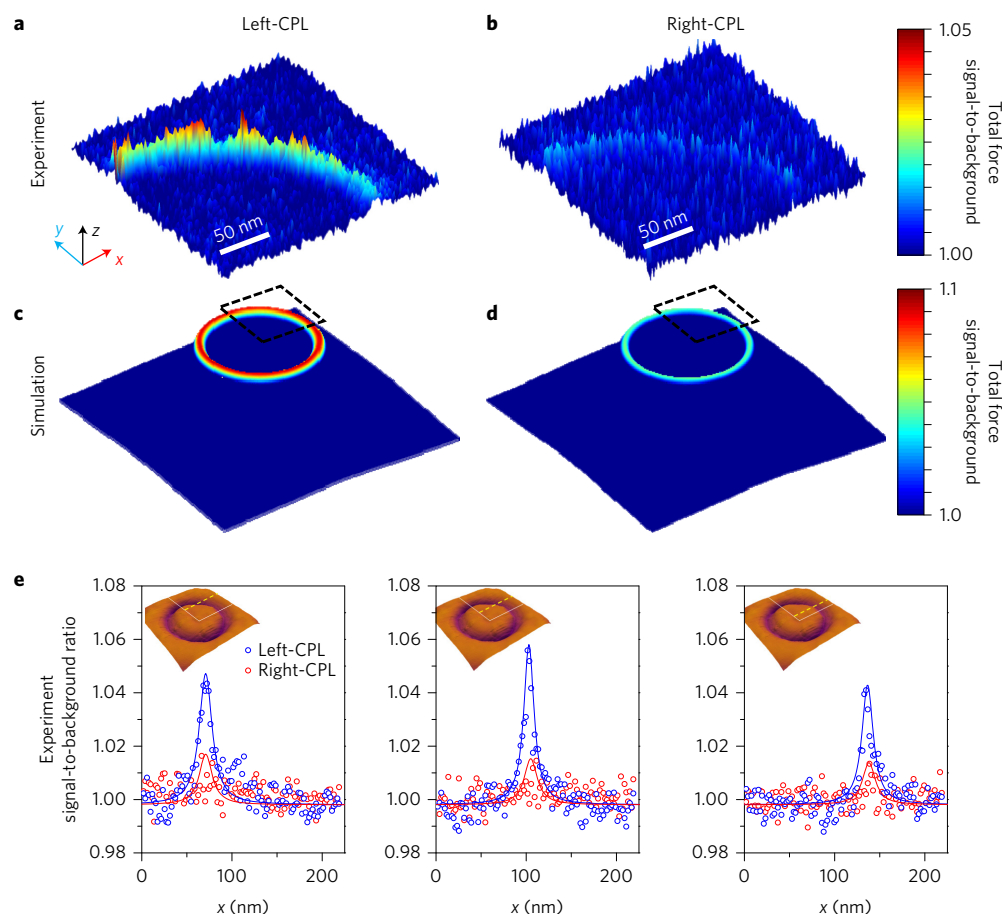
Figure 4 | Enantioselective optical force map. a, A quadrant of an experimental chiral force map on the coaxial nano-aperture with left-CPL illumination. **b**, Force map with the same chiral tip, but with right-CPL illumination. Both **a** and **b** show total forces normalized to the background signal and plotted in linear scale with ranges indicated in the colour bar to the right. **c,d**, Simulated optical forces with left-CPL (**c**) and right-CPL (**d**) illumination on the optical tweezer. The dashed square indicates the quadrant where the optical force map is experimentally measured. **e**, Normalized measured forces (signal-to-background ratio) in linear scale, along three horizontal locations across the coaxial aperture. The location of each line scan is indicated by the yellow dashed line in the inset, overlaid on the AFM topological map. White lines in the inset indicate the quadrant of the coaxial aperture where the optical force maps are taken.

respectively, give rise to attractive and repulsive trapping potentials (Fig. 3g).

Next, we leverage our high-resolution COFM technique to directly visualize enantioselective optical forces. By scanning the chiral tip over a quadrant of our optical tweezer while illuminating with left- or right-CPL, we create full two-dimensional force maps for each handedness with 2 nm spatial precision. Figure 4a,b show that the normalized optical force exerted with left-CPL (Fig. 4a) is substantially stronger than that with right-CPL (Fig. 4b), and FDTD simulations (Fig. 4c,d) corroborate this trend. These measurements confirm that the optical forces emanate from the dielectric channel of the coaxial aperture and not simply from the gold film. Note that each force map is normalized to the mean force measured across an area of 70×70 nm^2 on the gold film in the centre of the coaxial aperture, highlighting the favourable signal-to-background ratio afforded by this technique.

To further quantify the signal-to-background ratio for both CPL illumination conditions, we take individual one-dimensional line scans across the dielectric channel. Three representative line scans are shown in Fig. 4e for left-CPL (blue dots) and right-CPL (red dots). The positions of the scans are shown by dotted lines in the inset AFM topographical maps. As seen, near the aperture, the optical forces generated from left-CPL are three times stronger than those with right-CPL.

In summary, we have demonstrated a technique for enhancing and quantifying enantioselective optical forces. Using a chiral AFM probe to interrogate an achiral coaxial nano-aperture, we show that the optical forces are highly dependent on the handedness of the illumination as well as the chirality of the probe. Our control experiments with achiral probes demonstrate a negligible difference between the optical forces with left- and right-CPL illumination, confirming that the chirality-dependent optical forces arise both from the chirality of the probe as well as the local chirality density of the optical field. We envision that the capability to directly quantify and map piconewton chiral optical forces will enable new ways to study chiral materials and fields. For example, by functionalizing an achiral probe with a chiral molecule or nanoparticle, the optical forces exerted on that specimen could be measured. By monitoring changes in the force, conformational changes in the specimen might be detected in real time. Finally, measuring the force difference on enantiomeric pairs could lead to chiral sorting and optically controlled enantiopure chemical syntheses.

Methods

Methods and any associated references are available in the online version of the paper.

References

1. Canaguier-Durand, A., Hutchison, J. A., Genet, C. & Ebbesen, T. W. Mechanical separation of chiral dipoles by chiral light. *New J. Phys.* **15,** 123037 (2013).
2. Hayat, A., Mueller, J. P. B. & Capasso, F. Lateral chirality-sorting optical forces. *Proc. Natl Acad. Sci. USA.* **112,** 13190–13194 (2015).
3. Tkachenko, G. & Brasselet, E. Optofluidic sorting of material chirality by chiral light. *Nat. Commun.* **5,** 3577 (2014).
4. Wang, S. B. & Chan, C. T. Lateral optical force on chiral particles near a surface. *Nat. Commun.* **5,** 4307 (2014).
5. Robert, P. C., Stephen, M. B. & Alison, M. Y. Discriminatory optical force for chiral molecules. *New J. Phys.* **16,** 013020 (2014).
6. Noorduin, W. L. *et al.* Complete chiral symmetry breaking of an amino acid derivative directed by circularly polarized light. *Nat. Chem.* **1,** 729–732 (2009).
7. Yeom, J. *et al.* Chiral templating of self-assembling nanostructures by circularly polarized light. *Nat. Mater.* **14,** 66–72 (2015).
8. Berthelot, J. *et al.* Three-dimensional manipulation with scanning near-field optical nanotweezers. *Nat. Nanotech.* **9,** 295–299 (2014).
9. Grigorenko, A. N., Roberts, N. W., Dickinson, M. R. & Zhang, Y. Nanometric optical tweezers based on nanostructured substrates. *Nat. Photon.* **2,** 365–370 (2008).
10. Ndukaife, J. C. *et al.* Long-range and rapid transport of individual nano-objects by a hybrid electrothermoplasmonic nanotweezer. *Nat. Nanotech.* **11,** 53–59 (2016).
11. Righini, M., Volpe, G., Girard, C., Petrov, D. & Quidant, R. Surface plasmon optical tweezers: tunable optical manipulation in the femtonewton range. *Phys. Rev. Lett.* **100,** 186804 (2008).
12. Roxworthy, B. J., Bhuiya, A. M., Vanka, S. P. & Toussaint, K. C. Understanding and controlling plasmon-induced convection. *Nat. Commun.* **5,** 3173 (2014).
13. Shoji, T. & Tsuboi, Y. Plasmonic optical tweezers toward molecular manipulation: tailoring plasmonic nanostructure, light source, and resonant trapping. *J. Phys. Chem. Lett.* **5,** 2957–2967 (2014).
14. Bailey, J. *et al.* Circular polarization in star-formation regions: implications for biomolecular homochirality. *Science* **281,** 672–674 (1998).
15. Cronin, J. R. & Pizzarello, S. Enantiomeric excesses in meteoritic amino acids. *Science* **275,** 951–955 (1997).
16. Kuzyk, A. *et al.* Reconfigurable 3D plasmonic metamolecules. *Nat. Mater.* **13,** 862–866 (2014).
17. Alizadeh, M. H. & Reinhard, B. M. Transverse chiral optical forces by chiral surface plasmon polaritons. *ACS Photon.* **2,** 1780–1788 (2015).
18. Tang, Y. & Cohen, A. E. Enhanced enantioselectivity in excitation of chiral molecules by superchiral light. *Science* **332,** 333–336 (2011).
19. Lu, F., Jin, M. & Belkin, M. A. Tip-enhanced infrared nanospectroscopy via molecular expansion force detection. *Nat. Photon.* **8,** 307–312 (2014).
20. Munday, J. N., Capasso, F. & Parsegian, V. A. Measured long-range repulsive Casimir–Lifshitz forces. *Nature* **457,** 170–173 (2009).
21. de Man, S., Heeck, K. & Iannuzzi, D. Halving the Casimir force with conductive oxides: experimental details. *Phys. Rev. A* **82,** 062512 (2010).
22. Rajapakse, I., Uenal, K. & Wickramasinghe, H. K. Image force microscopy of molecular resonance: a microscope principle. *Appl. Phys. Lett.* **97,** 073121 (2010).
23. Huang, F., Tamma, V. A., Mardy, Z., Burdett, J. & Wickramasinghe, H. K. Imaging nanoscale electromagnetic near-field distributions using optical forces. *Sci. Rep.* **5,** 10610 (2015).
24. Nowak, D. *et al.* Nanoscale chemical imaging by photoinduced force microscopy. *Sci. Adv.* **2,** e1501571 (2016).
25. Saleh, A. A. E., Sheikhoelislami, S., Gastelum, S. & Dionne, J. A. Grating-flanked plasmonic coaxial apertures for efficient fiber optical tweezers. *Opt. Express* **24,** 20593–20603 (2016).
26. Van de Haar, M. A., Maas, R., Schokker, H. & Polman, A. Experimental realization of a polarization-independent ultraviolet/visible coaxial plasmonic metamaterial. *Nano Lett.* **14,** 6356–6360 (2014).
27. Zhao, Y., Saleh, A. A. E. & Dionne, J. A. Enantioselective optical trapping of chiral nanoparticles with plasmonic tweezers. *ACS Photon.* **3,** 304–309 (2016).
28. Lezec, H. J. *et al.* Beaming light from a subwavelength aperture. *Science* **297,** 820–822 (2002).
29. Hentschel, M., Schäferling, M., Weiss, T., Liu, N. & Giessen, H. Three-dimensional chiral plasmonic oligomers. *Nano Lett.* **12,** 2542–2547 (2012).
30. Bekshaev, A. Y. Subwavelength particles in an inhomogeneous light field: optical forces associated with the spin and orbital energy flows. *J. Opt.* **15,** 044004 (2013).

Author contributions

Y.Z. and J.A.D. conceived and designed the experiments. Y.Z., A.A.E.S. and M.A.v.d.H. performed the experiments. A.L. and O.A.R.-B. assisted with the experiments. Y.Z. and B.B. conducted the theory and numerical simulations. Y.Z., J.A.B. and J.A.D. co-wrote the paper. J.A.D. supervised the entire study. All authors contributed to the analysis of the data and revision of the paper.

Additional information

Supplementary information is available in the online version of the paper. Reprints and permissions information is available online at www.nature.com/reprints. Publisher's note: Springer Nature remains neutral with regard to jurisdictional claims in published maps and institutional affiliations. Correspondence and requests for materials should be addressed to Y.Z. and J.A.D.

Competing financial interests

The authors declare no competing financial interests.

Methods

Optical force measurement. The experimental schematic is presented in Supplementary Fig. 1, with additional detailed descriptions in Supplementary Note 1. Briefly, the AFM (Asylum Research MFP-3D Bio) was integrated with an inverted microscope (Zeiss, Axio Observer Z1m). The unit was mounted within a temperature- and vibration-control chamber, where a temperature-stabilized heat reservoir was set to be ∼5 °C above room temperature with a temperature precision of 0.1 °C, and equilibrated with the sample for 10 h before measurement. This set-up was used to minimize expansion and contraction of the sample and tip. A tunable laser source was fibre-coupled (multimode, Thorlabs) into the chamber and then collimated with a reflective collimator (RC08APC-P01, Thorlabs). CPL was created by passing the collimated beam through a linear polarizer (GT10-B Glan Taylor Polarizer, Thorlabs) and a quarter-wave plate (AQWP05M-600, Thorlabs). The laser beam was focused with a ×50 objective lens (NA = 0.55, Zeiss) onto the glass substrate with the coaxial nano-aperture.

During the force measurement, we first located a specific height above the surface by means of a force–distance curve. Then, at a designated height, we modulated the incident light through the coaxial aperture at a frequency that matched the cantilever's natural resonance (see Supplementary Fig. 2 and Supplementary Note 1 for more details of the measurement). The light was modulated with an acousto-optic modulator (AOMO 3110-191, Gooch & Housego), with the modulation signal connected to the reference of a lock-in amplifier (SRS 865, Stanford Research Systems). The cantilever deflection signal was routed from the AFM controller (ARC2) to the input of the lock-in amplifier. The measurement time frame was ∼5 min for mapping in Fig. 4 and ∼10 s for single point force measurements in Figs 2 and 3. An uncoated silicon AFM tip was used for achiral force measurements (PPP-FM, Nanosensors) with a spring constant of 1.44 nN nm^{-1} and a fundamental resonance at 64.167 kHz (shown in Fig. 3). Additional control experiments measured with a silicon tip, achiral and chiral gold-coated tips, and a chiral non-plasmonic tip under various illumination conditions are shown in Supplementary Notes 2–7.

Statistics of the measurements. All measurement data were scaled to an input intensity of 100 μW μm^{-2} for simplicity. Input intensity was monitored during the measurement with a beamsplitter, and the mean value of the input intensity was used in the normalization. The actual input intensities ranged from 18 μW μm^{-2} to 53 μW μm^{-2} during multiple sets of experiments. As shown in Fig. 3, randomly down-sampled raw data from the measurements are displayed, with the standard deviation and mean values calculated from all the raw data for each tip–aperture separation.

Coaxial nano-aperture fabrication and chiral tip fabrication. For the coaxial nano-aperture, we started with an optical flat glass substrate (C1737-1107, Delta Technologies). The substrate was first rinsed in deionized water and sonicated for 15 min, followed by a base piranha clean (5:1:1 = H_2O:NH_4OH:H_2O_2) for another 15 min at 65 °C, then dried with compressed air. After cleaning, a 50 nm layer of chromium was sputtered onto the substrate as a hard mask. Using focused ion beam (FIB) milling (Helios 660i, FEI) at 7.7 pA and 30 keV accelerating voltage, the peripheral grating was patterned into the glass coverslip, with a grating period of 500 nm and etching depth of 60 nm. After patterning, the chromium mask was removed by wet etching (Chromium Etchant 1020AC, Transene). Titanium (3 nm) and gold (220 nm) were subsequently sputtered on the sample. Finally, the coaxial aperture was fabricated at the centre of the grating by FIB milling (1 pA, 30 keV). The coaxial aperture had an inner diameter of 270 nm and an outer diameter of 330 nm, with a 6° tapering angle (from the ion beam).

For the chiral tip, gold-coated silicon cantilevers were commercially available (Nanosensors, PPP-FMAu) with the same spring constant and shape as the uncoated silicon cantilever. The gold coating was ∼35 nm thick (marked as t in the SEM in Fig. 3b) and uniformly covered the front and back sides of the cantilever. The nano-spiral pattern had 10 spiral periods and an edge-to-edge dimension of ∼2.5 μm. If fabricated on a planar surface, within one period, the gold spiral had a width of ∼74.2 nm and the gap between the gold spirals was ∼38.2 nm. We patterned this nano-spiral on the AFM tip with FIB milling (FEI Helios 660i), with a beam current of 1 pA and accelerating voltage of 30 kV for 1 min and 55 s. When the pattern was transferred to the AFM tip, the spiral period was elongated owing to the facet angle of the AFM tip, and the final period was ∼155 nm (marked p in Fig. 3b).

Data availability. The data that support the plots within this paper and other findings of this study are available from the corresponding authors upon reasonable request.